Available online at www.sciencedirect.com

ScienceDirect

IFAC PapersOnline CONFERENCE PAPER ARCHIVE

IFAC PapersOnLine 55-40 (2022) 55–60

Application of CFD in Control-Oriented Modeling of a DTB's Hydrodynamics ⋆

Jan M. Schaßberger * **Lutz Gröll** *

* *Karlsruhe Institute of Technology, Hermann-von-Helmholtz-Platz 1, 76344 Eggenstein-Leopoldshafen, Germany (e-mail: {jan.schassberger, lutz.groell}@kit.edu).*

Abstract: This contribution presents an application of the computational fluid dynamics (CFD) method in control-oriented modeling of a draft tube baffle (DTB) crystallizer's hydrodynamics. First, a CFD simulation of the overall system is performed. In a second step, the results of this simulation serve as basis for the comparison of partial DTB configurations with parts of our developed model, which is based on transport and transport-like partial differential equations (PDEs). Comparing the results of the PDE models with those of the transient CFD simulations allows an improvement of the developed hydrodynamic model and an assessment of the approximation quality. It is shown that the developed PDE models can represent the complex flow inside the DTB sufficiently well.

Keywords: Modeling, Model Comparison, Parameter Estimation, Computational Fluid Dynamics, Draft Tube Baffle Crystallizer

1. INTRODUCTION

Computational fluid dynamics (CFD) is a common method for the analysis and system design in many areas of science and industry. Besides the classical fields of application, CFD methods are also used for control-engineering purposes. Examples for the application in modeling include the estimation of model parameters of

- gray- and white-box models of air and water crafts (de Barros et al. (2004), Ramírez-Macías et al. (2016))
- black-box models of process engineering systems (Huisman (2005), Wu et al. (2019)), air crafts (Liu et al. (2015)), heating, ventilation and air conditioning systems (Zerihun Desta et al. (2004)) and flow control (Rizzo et al. (2006)).

Moreover, there are approaches for the direct use of CFD for controller design and testing in the fields of

- baking processes in Ousegui et al. (2012)
- civil engineering in Xiao et al. (2013)
- wind power plants in Fleming et al. (2016).

The authors are currently working on a control-oriented model of industrial-scale draft tube baffle (DTB) crystallizers, which shall serve as basis for the development of model-based controllers as demonstrated for other crystallizer types by Kleinert et al. (2010). Thus, in a first step a model of the hydrodynamics, accounting for the transport processes inside the plant, is developed. The model incorporating results of CFD simulations, published by ten Cate et al. (2000) and Wantha and Flood (2008), is based on transport and transport-like partial differential equations (PDEs), where by the latter we denote inhomogeneous transport PDEs. In this contribution, we present a comparison between the simulation results of our developed model and a conducted CFD study to asses the approximation quality and further improve our model. We use CFD for two main reasons. First, measurement of velocity and concentration distributions is difficult especially for large-scale industrial plants. Second, the determination of model parameters based on input-output measurement data is particularly challenging for crystallization processes as it is difficult to obtain representative and accurate measurement data due to internal segregation caused by particle-size dependent slip velocity (Eek (1995)). Moreover, plant-integrated online measurement devices for crystal size distributions are expensive, which is why many industrial plants are not equipped with such a device (Larsen et al. (2006)). Hence, identification is challenging and the evaluation of the control-oriented model using high-fidelity models, like ones based on CFD, is advantageous for the reduction of the size and/or dimension of the search space.

We first give a brief description of the DTB crystallization process in Section 2 and of our modeling approach in Section 3. Then, the CFD simulation results of the overall system are presented in Section 4. In Section 5, we compare the simulation results of our transport PDE models with those of CFD simulations of partial DTB configurations, derive improvements and draw conclusions about the model's applicability. The comparison is shown for two zones that have particularly complex hydrodynamics.

2. PROCESS DESCRIPTION

DTBs are used in various areas like the fertilizer industry and are built in different sizes up to several hundred cubic meters (Larsen et al. (2006), Beckmann (2013)). Inside the DTB a slurry, consisting of solvent, solute and solid crystals, circulates around a draft tube, as depicted in

⋆ The authors acknowledge support by the state of Baden-Württemberg through bwHPC.

10.1016/j.ifacol.2023.01.048

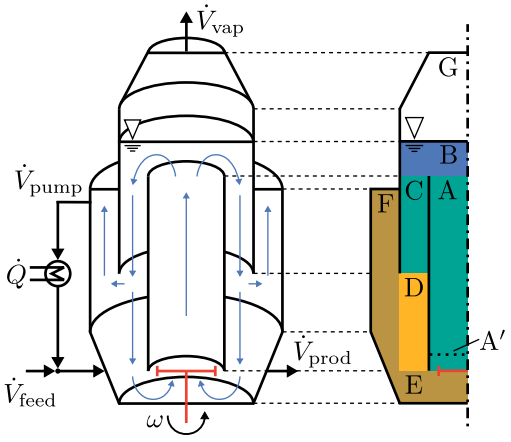

Fig. 1. Scheme of a DTB crystallizer and its internal (blue arrows) as well as external flows (black arrows) on the left and its segmentation for modeling on the right, impeller highlighted in red

the left half of Fig. 1. By shifting the thermodynamic equilibrium of the slurry's components, crystal growth and shrinkage can be achieved. When exceeding a certain level of supersaturation, which is generated through the evaporation of solvent, primary nucleation can occur, i.e., the formation of new crystals from solution. Besides primary nucleation, attrition and crystal breakage, e.g. due to collisions with the impeller, are an important source of nuclei (Mitrović (2002)). Due to a size-dependent slip velocity, crystals do not follow the liquid ideally. This is exploited in the settling zone, denoted by F in the right side of Fig. 1, so that small crystals leave the crystallizer towards the heat exchanger, where they partly dissolve (Eek (1995)). However, the large crystals remain inside the crystallizer and become increasingly bigger. Under operating conditions that aim to maximize the crystal size, a persistent oscillation of the size distribution occurs, which has been reported by numerous authors (Eek (1995), Mitrović (2002), Bermingham (2003)).

3. MODELING APPROACH

For the detailed modeling of flows, the Navier-Stokes equation is usually applied. However, this approach cannot be used with common model-based analysis and synthesis methods of control engineering. Thus, we use transport and transport-like PDEs as a compromise since they are of manageable complexity but also match the infinite dimensional nature of the system. To further simplify the modeling, we consider the flow inside the crystallizer to be symmetrical and divide the plant into several zones according to spatially occurring effects. These zones are shown on the right side of Fig. 1, where the different colors indicate zones with comparable behavior. Novel transport models are developed for the brown, orange and blue zones, whereas the well-known one-dimensional transport PDE is used for the green zones. The PDEs are coupled at their boundaries via mass flows. A detailed description will be published in Schaßberger and Gröll (2022).

4. CFD MODEL OF THE OVERALL PROCESS

As a first step, a CFD simulation of the overall DTB is performed. For this the geometry data published in Wantha and Flood (2008) of a DTB, which is approximately one cubic meter in size. A saturated ammonium sulfate-water solution at 80°C with a volume weighted mixing law for the density, but otherwise constant properties, is considered. The material parameters and process conditions are summarized in Table 1, where the latter are based on Wantha and Flood (2008). Since no data for the viscosity of saturated ammonium sulfate within the relevant temperature range was found in literature, the viscosity of 42% solution published in Eek (1995) is used, as the viscosity only depends slightly on the dissolved amount of ammonium sulfate. Similar to ten Cate et al. (2000) and Song et al. (2010), a marine-type impeller is used. Its geometry corresponds to Bermingham (2003), although in this study a scaled version is used due to the smaller diameter of the draft tube. For simulation, we use a multiple reference frame (MRF) approach combined with the widely-used standard k-ε model. The combination of both is common in the simulation of DTBs (Song et al. (2010), Pan et al. (2016)) and stirred baffled tanks (Vakili and Nasr Esfahany (2009), Li and Xu (2017)). Moreover, we use scalable wall functions and do not consider the gaseous phase, which is a frequently made assumption (ten Cate et al. (2000), Song et al. (2010)). The overall model consists of approximately 6.5 million cells. Ansys® Academic Research Fluent, Release 20.2 is used for simulation.

Fig. 2 shows the velocity magnitude inside the DTB. The interval of the velocity is truncated to 1.5 $\text{m}\cdot\text{s}^{-1}$ to increase the visibility of details in the flow around the draft tube. We generally observe good agreement with the results published in ten Cate et al. (2000), where a DTB of a similar size and substance-system was simulated. The results in Wantha and Flood (2008) cannot be used as a reference since they approximated the impeller by a momentum source, which yields a much more homogeneous flow. Due to the good agreement with the results in ten Cate et al. (2000), the simulation results are considered to be plausible.

5. MODEL COMPARISON

In the following, our models of the hydrodynamics are compared with results of transient CFD simulations. We focus on Zone A in Section 5.1 and Zone B in Section 5.2, as these have the most complex and inhomogeneous flow. Previously published literature, regarding the use of CFD

Table 1. Material and process parameters, 1: Eek (1995), 2: Bermingham (2003), 3: Wantha and Flood (2008).

Material parameter	Value	Unit	Reference
Density water	$1{\cdot}10^{3}$	$\text{kg}\cdot\text{m}^{-3}$	-
Density ammonium sulfate	$2.5{\cdot}10^{3}$	$\text{kg}\cdot\text{m}^{-3}$	1
Viscosity solution	$3.5{\cdot}10^{-3}$	Pa·s	1
Process parameter	**Value**	**Unit**	**Reference**
Number of fine outlets	2	-	3
Speed of rotation (ω)	320	rpm	2
Temperature of solution	80	°C	-
Mass share of solute	0.4848	-	2
$\dot{V}_{\text{prod}}$	0.18	$\text{kg}\cdot\text{s}^{-1}$	3
$\dot{V}_{\text{pump}}$ (per outlet)	0.5	$\text{kg}\cdot\text{s}^{-1}$	3
$\dot{V}_{\text{feed}}$	1.18	$\text{kg}\cdot\text{s}^{-1}$	3

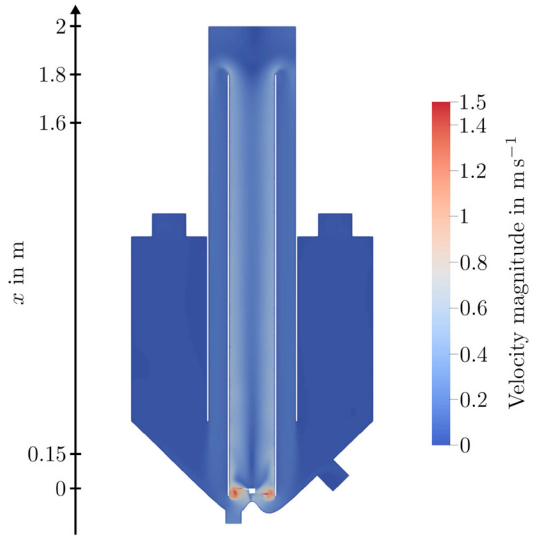

Fig. 2. Velocity magnitude inside the DTB (interval of velocity truncated to $1.5\,\mathrm{m{\cdot}s^{-1}}$)

for control-oriented modeling, usually utilizes the overall system input/output response for comparison and identification. Unfortunately, this approach is not promising in this application since the size of the plant and the process conditions would lead to high computational effort. Thus, we consider partial DTB configurations, which are initialized with velocity profiles obtained from the overall CFD simulation. This allows for a more time-efficient and detailed analysis of the model equations. As a consequence, the simulation results of the partial DTB simulations do not exactly match those of the overall simulation. However, from our point of view the accuracy is sufficient for evaluating the suitability of our PDE models as the partial configurations reflect the main characteristics of the flow.

5.1 Zone A - Flow Inside the Draft Tube

For modeling of zone A, an one-dimensional transport PDE of the volume fraction of the solute $\zeta_\mathrm{d}(t,x)$ is used. At the input boundary, $\zeta_{\mathrm{d,in}}(t)$ is calculated from

$$\zeta_{\mathrm{d,in}}(t) = \frac{\dot{m}_{\mathrm{d,in}}(t)\nu_\mathrm{d}}{\dot{m}_{\mathrm{d,in}}(t)\nu_\mathrm{d} + \dot{m}_{\mathrm{w,in}}(t)\nu_\mathrm{w}}, \tag{1}$$

where ν denotes the specific volume of solvent (index w) and solute (index d) and $\dot{m}(t)$ their mass flows. The transport PDE is given by

$$\begin{aligned} &\frac{\partial \zeta_\mathrm{d}(t,x)}{\partial t} + v(t)\,\frac{\partial \zeta_\mathrm{d}(t,x)}{\partial x} = 0, \qquad (2)\\ &\text{IC}: \ \zeta_\mathrm{d}(t_0,x) = \zeta_{\mathrm{d},0}(x),\\ &\text{BC}: \ \zeta_\mathrm{d}(t,0) = \zeta_{\mathrm{d,in}}(t), \end{aligned}$$

where $t \geq t_0$, $x \in [0,\,\ell]$, $v(t)$ denotes the velocity of the solution and ℓ the vertical length of zone A. The mass flow of both components at the output boundary can be calculated from

$$\dot{m}_\mathrm{w}(t) = A\rho_\mathrm{w}\zeta_\mathrm{w}(t,\ell)v(t), \tag{3a}$$
$$\dot{m}_\mathrm{d}(t) = A\rho_\mathrm{d}\zeta_\mathrm{d}(t,\ell)v(t). \tag{3b}$$

Here, A denotes the cross sectional area of the draft tube and ρ the component's densities. For comparison of the CFD simulations and the developed models, the mass share of ammonium sulfate $w_\mathrm{d}(t)$ is considered, which can be calculated from

$$w_d(t,\ell) = \frac{\dot{m}_\mathrm{d}(t,\ell)}{\dot{m}_\mathrm{w}(t,\ell) + \dot{m}_\mathrm{d}(t,\ell)}. \tag{4}$$

When developing the segmentation of the DTB, the entire volume inside the draft tube was considered as one zone. However, the overall CFD simulation shows that there is a vortex above the impeller as depicted in Fig. 3. Thus, the initial segmentation needs to be reconsidered. As the flow above the vortex is quite homogeneous, the original model is applied for the flow starting 15 cm above the impeller, as illustrated by A' in Fig. 1. In the following, we limit our considerations to this area. A better approximation of the volume including the impeller and the vortex in the first 15 cm might be an ideally mixed volume, but this needs to be confirmed by further analysis.

In Fig. 4, the CFD simulation of the overall plant and that of the partial DTB configuration are compared. The latter are obtained from a transient simulation using a comparable mesh size and otherwise unchanged conditions. There is a good overall agreement between both velocity contours. Only the velocity in the center of the draft tube is slightly smaller for the partial DTB configuration.

For comparing our approach of zone A, given by (1–3), and the CFD simulation of the partial DTB configuration, a five percent decrease in concentration of ammonium sulfate at $t = 0\,\mathrm{s}$ is considered. For the transport PDEs, an averaged fluid velocity $v(t) = \dot{V}(t)/A$ is used, where $\dot{V}(t)$ is the volume flow of solution and A the cross sectional area. In this simulation, however, the volume flow is kept constant. In Fig. 5 the mass share of ammonium sulfate at the output boundary is shown for both models. One can see that the non-homogeneous velocity profile, included in the CFD simulation, leads to a softening of the change in concentration at the input boundary, while the transport PDE model preserves the step-like change. The maximum relative error is about six percent.

To achieve a more accurate approximation of the flow, a radius-dependent velocity distribution $v(t,r) = arv(t) + v_0$ with v_0, $a > 0$ seems promising. The related PDE is given

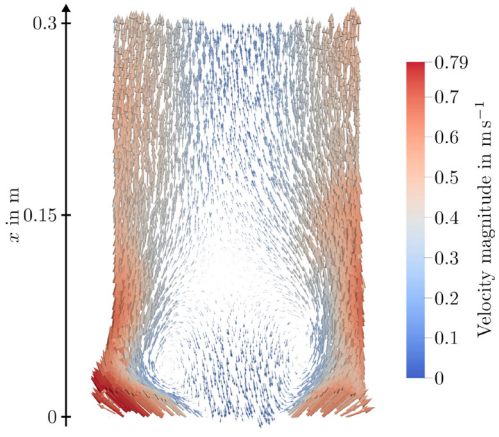

Fig. 3. Tangential projection of the velocity vectors, position indication relative to the impeller

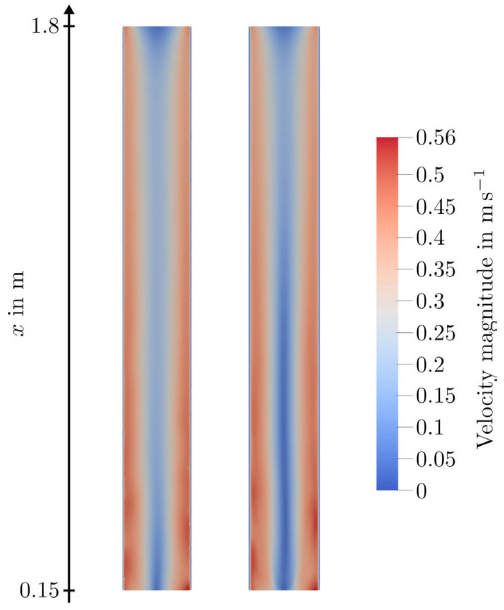

Fig. 4. Comparison of the velocity profile of the overall CFD simulation (left) and that of the partial DTB configuration (right), position indication relative to the impeller

for $t \geq t_0$, $r \in [0,\, r_\mathrm{i}]$, $x \in [0,\, \ell]$ by

$$\begin{aligned} &\frac{\partial \zeta_\mathrm{d}(t,r,x)}{\partial t} + v(t,r)\,\frac{\partial \zeta_\mathrm{d}(t,r,x)}{\partial x} = 0, \qquad (5)\\ &\text{IC}: \;\; \zeta_\mathrm{d}(t_0,r,x) = \zeta_{\mathrm{d},0}(r,x),\\ &\text{BC}: \;\; \zeta_\mathrm{d}(t,r,0) = \zeta_{\mathrm{d,in}}(t), \end{aligned}$$

where (1) again is used for the calculation of $\zeta_{\mathrm{d,in}}(t)$. The mass flows at the output boundary are determined by

$$\dot{m}_\mathrm{w}(t) = \int_0^{r_\mathrm{i}} 2\pi r \rho_\mathrm{w} \zeta_\mathrm{w}(t,r,\ell) v(t,r)\,\mathrm{d}r, \qquad (6a)$$

$$\dot{m}_\mathrm{d}(t) = \int_0^{r_\mathrm{i}} 2\pi r \rho_\mathrm{d} \zeta_\mathrm{d}(t,r,\ell) v(t,r)\,\mathrm{d}r, \qquad (6b)$$

where r_i denotes the inner diameter of the draft tube. Using this approach, much better agreement with the results of the CFD simulation can be found as shown in Fig. 5. The parameters of the velocity distribution a, v_0 are determined by a parameter optimization using a quadratic cost function of the difference in solute concentration $w_\mathrm{d}(t)$ at the output boundary. The maximum relative error is less than two percent. Despite the better agreement of this

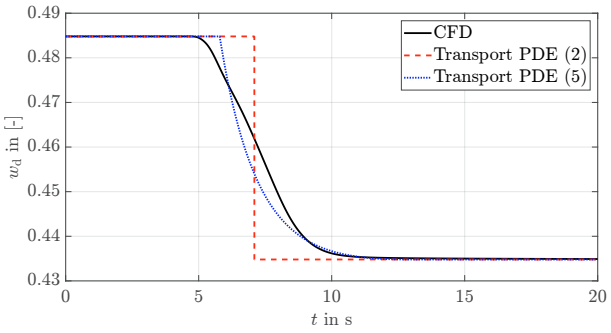

Fig. 5. Comparison of the mass share of ammonium sulfate at zone A's output boundary of the transient CFD simulation and the transport PDE models for a decrease in concentration by 5% at $t = 0\,\mathrm{s}$.

model, we currently prefer the simpler one (1–3) in view of the future development of the model by considering an additional solid phase.

5.2 Zone B - Flow Above the Draft Tube

For zone B, we developed a novel transport-like PDE with time- and radius-dependent length $\ell(t,r)$. This should describe the flow redirection and the fact that a particle starting in zone B close to the draft tube's edge leaves the zone earlier compared to a particle close to the draft tube's center, as this particle has to travel a longer distance. The states of the PDEs are the mass of the components per radius and length denoted by $\xi_\mathrm{w}(t,r,x)$ and $\xi_\mathrm{d}(t,r,x)$. At the input boundary, $\xi_{\mathrm{w,in}}(t,r)$ and $\xi_{\mathrm{d,in}}(t,r)$ are calculated from the following equations

$$\xi_{\mathrm{w,in}}(t,r) = \frac{2r\dot{m}_{\mathrm{w,in}}(t)}{r_\mathrm{i}^2 v(t)}, \qquad (7a)$$

$$\xi_{\mathrm{d,in}}(t,r) = \frac{2r\dot{m}_{\mathrm{d,in}}(t)}{r_\mathrm{i}^2 v(t)}. \qquad (7b)$$

The PDE of the local solvent density $\xi_\mathrm{w}(t,r,x)$ is given by

$$\begin{aligned} &\frac{\partial \xi_\mathrm{w}(t,r,x)}{\partial t} + v(t)\,\frac{\partial \xi_\mathrm{w}(t,r,x)}{\partial x} = -\dot{\mu}_\mathrm{v}(t), \qquad (8a)\\ &\text{IC}: \;\; \xi_\mathrm{w}\left(t_0,r,x\right) = \xi_{\mathrm{w},0}\left(r,x\right),\\ &\text{BC}: \;\; \xi_\mathrm{w}\left(t,r,0\right) = \xi_{\mathrm{w,in}}\left(t,r\right), \end{aligned}$$

and that of the solute's density $\xi_\mathrm{d}(t,r,x)$ by

$$\begin{aligned} &\frac{\partial \xi_\mathrm{d}(t,r,x)}{\partial t} + v(t)\,\frac{\partial \xi_\mathrm{d}(t,r,x)}{\partial x} = 0, \qquad (8b)\\ &\text{IC}: \;\; \xi_\mathrm{d}\left(t_0,r,x\right) = \xi_{\mathrm{d},0}\left(r,x\right),\\ &\text{BC}: \;\; \xi_\mathrm{d}\left(t,r,0\right) = \xi_{\mathrm{d,in}}\left(t,r\right), \end{aligned}$$

where $t \geq t_0$, $r \in [0,\, r_\mathrm{i}]$, $x \in \left[0,\, \ell(t,r)\right]$. The term $\dot{\mu}_\mathrm{v}(t)$ represents the evaporation of solvent close to the liquid surface and is considered to be zero in the following, as is the derivative of the zone's length $\dot{\ell}(t,r)$. Due to the radius-dependent length, the mass flows at the output boundary are given by

$$\begin{aligned} \dot{m}_\mathrm{w}(t,\ell(t,r)) = \int_0^{r_\mathrm{i}} &\Big(v(t) - \dot{\ell}(t,r)\Big) \\ &\cdot \xi_\mathrm{w}(t,r,\ell(t,r))\,\mathrm{d}r, \end{aligned} \qquad (9a)$$

$$\begin{aligned} \dot{m}_\mathrm{d}(t,\ell(t,r)) = \int_0^{r_\mathrm{i}} &\Big(v(t) - \dot{\ell}(t,r)\Big) \\ &\cdot \xi_\mathrm{d}(t,r,\ell(t,r))\,\mathrm{d}r. \end{aligned} \qquad (9b)$$

In this contribution, a linear relation of the length $\ell(t,r)$ is considered. The parameters of this length distribution need to be determined in such a way that the volume related to the domain of the PDE matches the physical liquid volume even with changes in the liquid level (Schaßberger and Gröll (2022)). However, according to the model idea, the parameters should be chosen such that $\ell(t,r)$ is a positive, monotonically decreasing function w.r.t. r.

Fig. 6 shows the result of the overall CFD simulation and that of the partial DTB configuration. Clearly, one can see deviations between the velocity contours. In case of the overall simulation, the flow velocity significantly decreases while deflection, whereas the velocity remains comparatively high in case of the approximation. However, the qualitative behavior like the formation of a vortex at the outer edge of the draft tube and the inhomogeneous

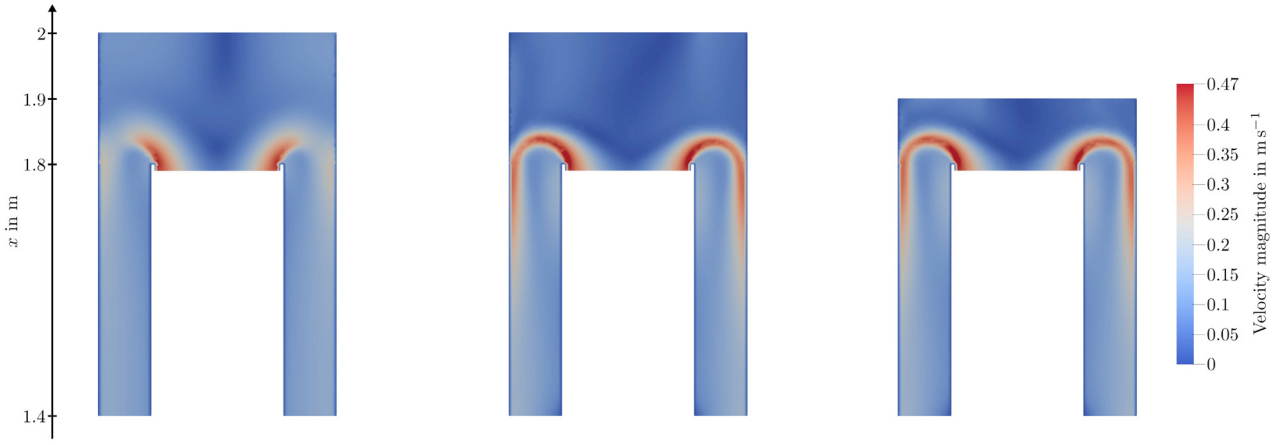

(a) Overall DTB (b) Partial DTB configuration (c) Partial DTB configuration with reduced liquid level

Fig. 6. Comparison of the velocity contours of the overall CFD simulation (a), the partial DTB configuration (b) and the partial DTB configuration with reduced liquid level (c), position indication relative to the impeller

velocity in the deflection and at the interface of the zones is reproduced well by the partial DTB configuration.

To compare the CFD simulation and the transport PDE model, we again consider a reduction of the ammonium sulfate's mass share of 5% at $t = 0\,\mathrm{s}$ and use the same approach to calculate the velocity of the transport models. For determination of the free parameter of $\ell(t, r)$, again a parameter optimization based on the mass share of the solute at the output boundary is performed. The results are shown in Fig. 7. One can see good overall agreement between the results of the CFD simulation of the partial DTB configuration and that of the proposed transport PDE model. When taking a closer look at the velocity vector field, shown in Fig. 8, we identify two issues

(1) A significant share of zone B's volume hardly interacts with the entering fluid. This causes the concentration at zone B's output to remain slightly above the new input concentration for a long time after an initial rapid drop. This can be observed in Fig. 7.
(2) A vortex at the zone B's outlet continuously carries higher concentrated solution over the boundary, which falsifies the results obtained from the CFD simulation.

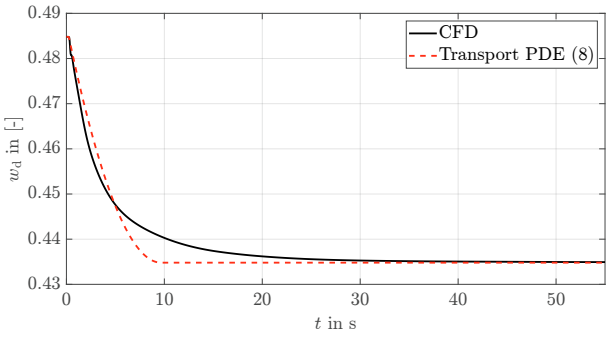

Fig. 7. Comparison of the mass share of ammonium sulfate at zone B's output boundary of the transient CFD simulation and the transport PDE model for a decrease in concentration by 5% at $t = 0\,\mathrm{s}$

Based on these observations, we conclude that the zone's boundary needs to be relocated to include the vortex. Moreover, we expect better agreement of our approach for DTBs with a smaller liquid column above the draft tube as the volume behaves more homogeneously. To verify these conclusions, a new CFD simulation of a partial DTB configuration with a reduced liquid column but otherwise unchanged conditions is performed. The resulting velocity contour is depicted in Fig. 6c. Comparing these results with Fig. 6b, it can be seen that the velocity contour changes only slightly despite the reduced liquid level.

When comparing the mass share of ammonium sulfate at the output boundary for the reduced liquid level, as shown in Fig. 9, with that in Fig. 7, one can see that the shape of the graph for $t \in [0\,\mathrm{s}, 10\,\mathrm{s}]$ changes and the decay of the change in concentration is achieved much faster although the zone's boundary is moved and thus the distance between the input and output is increased. Also in this case, the results of the transport PDEs show good agreement with that of the CFD simulation and the maximum relative error is less than one percent.

One possibility to reproduce the slow decay of the concentration in case of a high liquid level could be the division of zone B into two subzones. The flow diversion close to

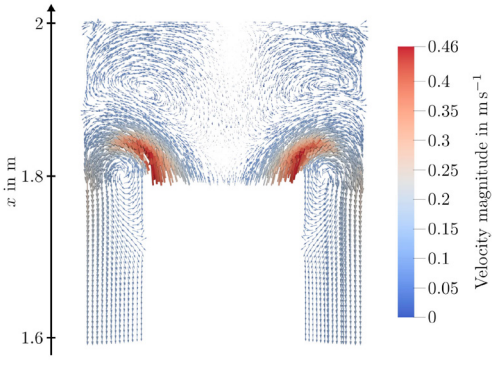

Fig. 8. Tangential projection of the velocity vectors in Zone B, position indication relative to the impeller

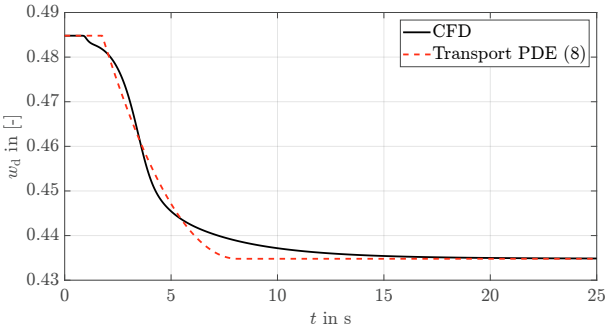

Fig. 9. Comparison of the mass share of ammonium sulfate at the zone's output boundary of the transient CFD simulation and the transport PDE model for zone B with reduced liquid level and a decrease in concentration by 5% at $t = 0\,\mathrm{s}$

the draft tube could be described by the developed model, while the resting liquid could be described by an ideally mixed volume coupled with the transport PDE via sink and source terms.

6. CONCLUSION

In the contribution, we have performed a CFD simulation of a DTB crystallizer. The results of the overall simulation have been used for the closer analysis of partial DTB configurations and their comparison with a developed hydrodynamics model based on transport and transport-like PDEs. Due to the comparison, we have been able to improve the segmentation of our control-oriented model and show good overall agreement between the adapted transport PDE models and the CFD results.

REFERENCES

Beckmann, W. (ed.) (2013). *Crystallization: Basic Concepts and Industrial Applications*. Wiley-VCH, Weinheim.

Bermingham, S. (2003). *A Design Procedure and Predictive Models for the Solution Crystallization Processes*. Ph.D. thesis, Delft University of Technology.

de Barros, E., Pascoal, A., and de Sa, E. (2004). AUV Dynamics: Modelling and Parameter Estimation Using Analytical, Semi-Empirical, and CFD Methods. *IFAC Proceedings Volumes*, 37(10), 369–376.

Eek, R. (1995). *Control and Dynamic Modelling of Industrial Suspension Crystallizers*. Ph.D. thesis, Delft University of Technology.

Fleming, P., Aho, J., Gebraad, P., Pao, L., and Zhang, Y. (2016). Computational Fluid Dynamics Simulation Study of Active Power Control in Wind Plants. In *2016 American Control Conference (ACC)*, 1413–1420.

Huisman, L. (2005). *Control of Glass Melting Processes Based on Reduced CFD Models*. Ph.D. thesis, Eindhoven University of Technology.

Kleinert, T., Weickgenannt, M., Judat, B., and Hagenmeyer, V. (2010). Cascaded Two-Degree-of-Freedom Control of Seeded Batch Crystallisations Based on Explicit System Inversion. *Journal of Process Control*, 20(1), 29–44.

Larsen, P., Patience, D., and Rawlings, J. (2006). Industrial Crystallization Process Control. *IEEE Control Systems Magazine*, 26(4), 70–80.

Li, L.C. and Xu, B. (2017). CFD Simulation of Floating Particles Suspension in a Stirred Tank. *Chem. Pap.*, 71, 1377–1387.

Liu, K., Da Ronch, A., Li, D., and Xiang, J. (2015). Modeling of Unsteady Aerodynamics for a Flapping Wing. *IFAC-PapersOnLine*, 48(28), 404–408.

Mitrović, A. (2002). Population Balance Based Modeling, Simulation, Analysis and Control of Crystallization Processes. In *Progress Reports VDI*, volume 749 of *Series 3: Process Engineering*. VDI Verlag.

Ousegui, A., Moresoli, C., Dostie, M., and Marcos, B. (2012). Optimal Control and CFD Modeling for Heat Flux Estimation of a Baking Process. *Computers & Chemical Engineering*, 38, 139–150.

Pan, H., Li, J., Jin, Y., Yang, B., and Li, X. (2016). Numerical Investigation of the Effect of Bottom Shape on the Flow Field and Particle Suspension in a DTB Crystallizer. *International Journal of Chemical Engineering*, 2016, 6862152.

Ramírez-Macías, J., Brongers, P., Rúa, S., and Vásquez, R. (2016). Hydrodynamic Modelling for the Remotely Operated Vehicle Visor3 Using CFD. *IFAC-PapersOnLine*, 49(23), 187–192.

Rizzo, M., Santillo, M., Padthe, A., Hoagg, J., Akhtar, S., Powell, K., and Bernstein, D. (2006). CFD-Based Adaptive Flow Control Using ARMARKOV Disturbance Rejection. In *2006 American Control Conference*, 3783–3788.

Schaßberger, J. and Gröll, L. (2022). Block-Oriented Modeling of a DTB Crystallizer's Hydrodynamics.

Song, X., Zhang, M., Wang, J., Li, P., and Yu, J. (2010). Optimization Design for DTB Industrial Crystallizer of Potassium Chloride. *Industrial & Engineering Chemistry Research*, 49(21), 10297–10302.

ten Cate, A., Bermingham, S., Derksen, J., and Kramer, H. (2000). Chapter 32 - Compartmental Modeling of an 1100L DTB Crystallizer Based on Large Eddy Flow Simulation. In H. van den Akker and J. Derksen (eds.), *10th European Conference on Mixing*, 255–264. Elsevier Science, Amsterdam.

Vakili, M. and Nasr Esfahany, M. (2009). CFD Analysis of Turbulence in a Baffled Stirred Tank, a Three-Compartment Model. *Chemical Engineering Science*, 64(2), 351–362.

Wantha, W. and Flood, A. (2008). Numerical Simulation and Analysis of Flow in a DTB Crystallizer. *Chemical Engineering Communications*, 195(11), 1345–1370.

Wu, Z., Tran, A., Ren, Y., Barnes, C., Chen, S., and Christofides, P. (2019). Machine Learning-Based Model Predictive Control of Distributed Chemical Processes. *IFAC-PapersOnLine*, 52(2), 120–127.

Xiao, H., Feng, L., and Zhi, Y. (2013). Tuning the PID Parameters for Greenhouse Control Based on CFD Simulation. In *2013 Second International Conference on Agro-Geoinformatics (Agro-Geoinformatics)*, 485–489.

Zerihun Desta, T., Janssens, K., Van Brecht, A., Meyers, J., Baelmans, M., and Berckmans, D. (2004). CFD for Model-Based Controller Development. *Building and Environment*, 39(6), 621–633.